atmosphere

Article

Spatial–Temporal Distribution of Tropospheric Specific Humidity in the Arid Region of Northwest China

Hao Zhang [1], Meiping Sun [1,2,*], Xiaojun Yao [1], Zhilan Wang [1] and Lei Zhang [1]

1 College of Geography and Environment Sciences, Northwest Normal University, Lanzhou 730070, China; zhanghao1996n@163.com (H.Z.); yaoxj_nwnu@163.com (X.Y.); wzl1997hh@163.com (Z.W.); zhlei6@163.com (L.Z.)

2 Northwest Institute of Eco-Environment and Resources, University of Chinese Academy of Sciences, Lanzhou 730000, China

* Correspondence: sunmeiping1982@nwnu.edu.cn

Abstract: Based on the atmospheric temperature and dew point temperature difference series of mandatory levels in the arid region of northwest China, we calculated the specific humidity of stations at 200, 300, 400, 500, 700, and 850 hPa and analyzed the spatial and temporal distribution. The specific humidity of radiosonde is compared with two sets of reanalysis data (ERA-interim from European Centre for Medium Range Weather Forecasts and Modern Era Retrospective Analysis for Research and Applications: MERRA-2). The annual specific humidity and summer specific humidity show a positive trend in the vertical atmospheric levels during the period 1958–2018. Taking the middle of the 1980s and 2002 as boundaries, the selected levels show the trend of "declining-gentle rising-fluctuation rising". The maximum specific humidity is observed at the level of 850–700 hPa during the warm months of the year, and the most vertical expansion in specific humidity is in July. In terms of spatial distribution, the specific humidity is greatly influenced by the topography and underlying surface at lower levels. The characteristics of spatial distribution of the trend are well described by the two sets of reanalysis data in the middle and upper levels, but there are some deficiencies in depicting the trend in the lower levels.

Keywords: Northwest China; troposphere; specific humidity; spatial and temporal distribution

check for updates

Citation: Zhang, H.; Sun, M.; Yao, X.; Wang, Z.; Zhang, L. Spatial–Temporal Distribution of Tropospheric Specific Humidity in the Arid Region of Northwest China. *Atmosphere* **2021**, *12*, 349. https://doi.org/10.3390/atmos12030349

Academic Editor: Yoshihiro Tomikawa

Received: 14 January 2021
Accepted: 1 March 2021
Published: 7 March 2021

1. Introduction

Water vapor in the atmosphere is the material basis for the formation of clouds and precipitation. Although water vapor accounts for only 1.53% of the total water volume in the global hydrological cycle system, it is the most active factor in the global water cycle, contributing to the global energy cycle through water vapor transport, water vapor convergence and divergence, water vapor budget, and water balance under the action of atmospheric circulation [1,2]. In recent years, due to an increase of greenhouse gases, global warming has intensified and atmospheric humidity has increased. Water vapor is itself a greenhouse gas, which has enhanced the warming effect caused by carbon dioxide and increased the water vapor feedback [3]. Humidity, an important physical parameter to characterize the water vapor content, can be characterized in many ways, such as mixing ratio, specific humidity, absolute humidity, relative humidity, dew point temperature, etc. Specific humidity is the ratio of mass between water vapor and total air in a cloud of moist air. If there is no mass exchange between wet air and the outside world and no phase change in wet air, specific humidity remains unchanged. In addition, specific humidity cannot be affected by pressure change, so it is commonly used to characterize and calculate atmospheric water vapor content [4–9]. Moreover, specific humidity is frequently used as a parameter to calculate water vapor transport flux, water vapor transport flux divergence, water vapor budget, and latent heat flux in the atmosphere [10–16]. Therefore, analyzing tropospheric specific humidity is beneficial for deepening the knowledge of climate change, providing a foundation for analyzing regional water vapor content, water vapor budget, and other factors, as well as providing a basis for coping with regional climate change and improving the accuracy of forecasting and early warning.

Scholars have conducted studies on the tropospheric specific humidity. Dessler et al. [17] found that specific humidity usually increases with short-term climate change (e.g., El Niño) based on five sets of reanalysis data: National Centers for Environmental Prediction/National Center for Atmospheric Research (NCEP/NCAR), ERA-40 reanalysis, Japanese Reanalysis (JRA), Modern Era Retrospective Analysis for Research and Applications (MERRA), and European Centre for Medium Range Weather Forecasts (ECMWF)-interim. Darand et al. [18] analyzed the distribution and variation of specific humidity of the troposphere 1000–500 hPa over Iran using ERA-interim reanalysis gridded data from 1979–2016. Zhang et al. [19] compared the differences between radiosonde and reanalysis data in terms of multi-year averages, annual variability, dispersion, and long-term trend based on four sets of reanalysis data and 850–300 hPa atmospheric specific humidity data of 118 radiosonde stations in China from 1979 to 2015. Guo et al. [20] studied the changes in the upper-air specific humidity during the period 1958–2005 by analyzing a time series of homogenized radiosonde dew point data from 92 selected stations in China. Xu et al. [21] mainly analyzed the temporal change characteristics of tropospheric specific humidity upon the middle-lower reaches of the Heihe River during the period 1981–2010 and found that the annual and seasonal specific humidity at the mandatory levels of 700 hPa, 500 hPa, and 200 hPa had first risen and then dropped, experiencing the "dry-wet-dry" process. Liu et al. [22] analyzed the temporal and spatial change characteristics of free atmospheric specific humidity as well as the relationship between humidity and surface temperature and precipitation during the period 1971–2005. In summary, the research of tropospheric specific humidity is usually based on two types of data: radiosonde data and reanalysis data. The former is important for the study of climate change due to its long monitoring time series, but there are a variety of problems of inaccurate observation data caused by instrument type change, inconsistent observation specifications, and station migration. The availability of reanalysis data provides an important source of information for revealing the patterns of atmospheric circulation, understanding the causes and mechanisms of climate change, and assessing the water cycle and energy balance, especially in areas where stations are sparse and unevenly distributed. Because of the instrument type change of the radiosonde data in China, humidity sensor shows that the humidity has abnormally dropped since 2006 in the arid region of northwest China. Therefore, it is necessary to correct and interpolate the specific humidity of radiosonde stations after 2006. The evaluation results found that the reanalysis data correlated well with the radiosonde data, so we corrected the specific humidity of radiosonde stations and constructed a long time series of specific humidity data sets for the period 1958–2018. In this paper, the spatial and temporal trend of specific humidity are analyzed based on radiosonde data and reanalysis data (ERA-interim and MERRA-2). Meanwhile, we assess the applicability of reanalysis data in the arid region of northwest China, which provides implications for the use of reanalysis data to analyze specific humidity and other elements in unevenly distributed and sparse areas in China. The paper is organized as follows. Section 2 shows the study area. Section 3 presents the description of the data sets and methodology. Section 4 analyzes the data and draw conclusions.

2. Data and Methods

2.1. Study Area

The arid region of northwest China (Figure 1), which is located between 73°–107° E and 34°–50° N, includes all of Xinjiang, western Inner Mongolia, and most of Gansu. The west side is Central Asia and the north side is connected with Mongolia and Russia. The south side is the Tibetan plateau, boarded by the Kunlun Mountains, the Altun Mountains, and the Qilian Mountains, and the eastern boundary is the Helan Mountains. The study area has a vast territory, with a distribution of plateaus, mountains, and basins; the terrain fluctuates greatly. There are many rivers and lakes in the region, such as the Tarim River, the Heihe River, the Irtysh River, the Manas Lake, the Bosten Lake, and so on, which are mostly supplied by the melting water of mountain ice and snow, and most of them dry up for a long time during the year. The spatial and temporal distribution of water resources is uneven. Due to its location in the interior of the continent and influenced by the dynamic and thermal factors of the Tibetan Plateau, the study area has less precipitation, with an annual mean precipitation of about 230 mm. The vegetation coverage is low, with the features of weak regeneration capacity and fragile ecological environment. However, the arid region of northwest China is seen, in the 21st century, as a valuable resource and contains energy strategic highlands, and is rich in wind energy and mineral and tourism resources. Moreover, it is a bridge to Central Asia and a key zone of "The Silk Road" [23–26].

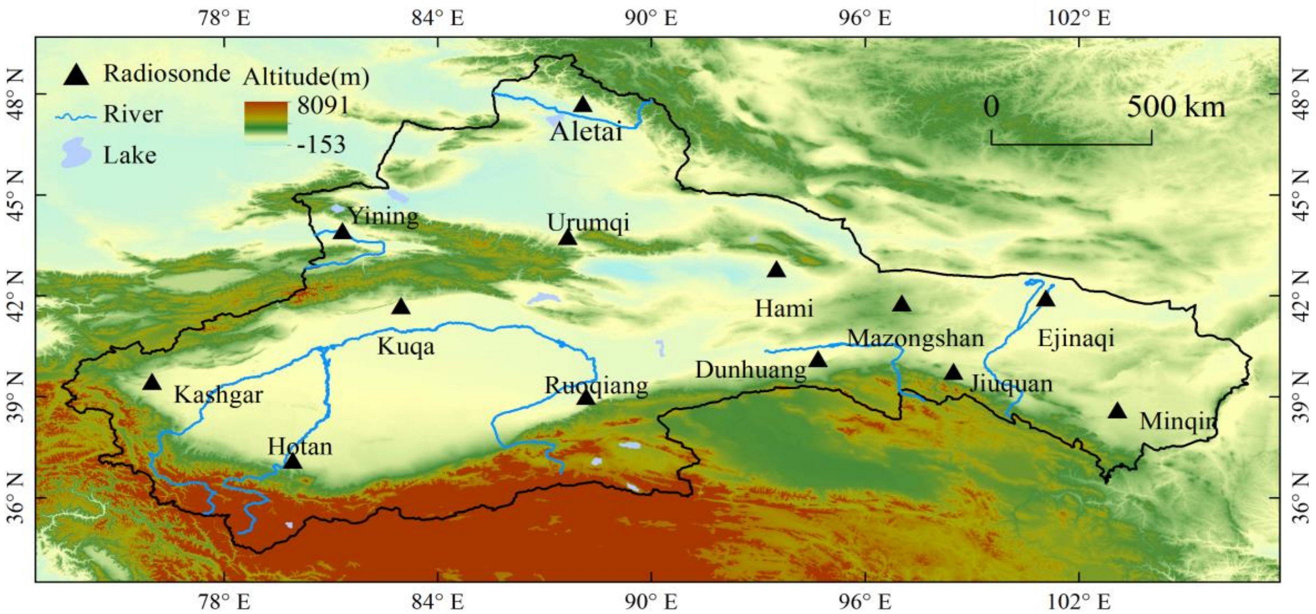

Figure 1. Location of the study region and distribution of radiosonde stations.

2.2. Data

The radiosonde data used in this study was downloaded from "Data Set of Monthly Values for China's Upper Specified Levels" in the China Meteorological Data Service Center (http://data.cma.cn accessed on 1 September 2020), which contained the monthly data of the mandatory levels of 88 stations during the period 1951–2014 in China, including atmospheric pressure (hPa), altitude (geopotential meters), temperature (0.1 °C), dew point temperature difference (0.1 °C), and wind speed (0.1 m/s). There were 17 levels, which have passed a series of quality control measures such as statistical and statics inspection. We chose six vertical pressure levels (200, 300, 400, 500, 700, 850 hPa), including temperature, altitude and dew point temperature difference observed month by month at 0000 UTC and 1200 UTC at each level. In this study, thirteen radiosonde stations, from 1958 to 2013, located in the arid region of northwest China, were finally selected (Figure 1).

The ERA-interim reanalysis data released by the European Centre for Medium-Range Weather Forecasts (ECMWF) (https://apps.ecmwf.int/datasets/data/interim-full-daily accessed on 1 September 2020) included the climatic elements of specific humidity, relative humidity, temperature, atmospheric pressure, etc., between January 1979 and December 2018. The horizontal resolution was increased to T255 with 37 vertical levels from 1000 hPa to 1 hPa; six of these levels (same as radiosonde stations) were selected to analyze specific humidity, with a temporal resolution of months and a spatial resolution of 0.75° × 0.75° [27].

The Modern-Era Retrospective Analysis data version 2 (MERRA-2), the latest atmospheric reanalysis of the modern satellite era produced by NASA's Global Modeling and

Assimilation Office (https://disc.gsfc.nasa.gov accessed on 1 September 2020), is mainly used for climate monitoring. MERRA-2, produced with version 5.12.4 of the Goddard Earth Observing System (GEOS) atmospheric data assimilation system, and M2I3NPASM-Assimilated Meteorological Fields were used in this study. The climatic elements included temperature, specific humidity, relative humidity, wind speed, net radiation, etc. The horizontal resolution had 42 vertical levels; six of these levels (same as radiosonde stations), between January 1980 and December 2018, were selected to analyze specific humidity, with a temporal resolution of months and a spatial resolution of 0.5° × 0.625° [28,29].

2.3. Methods

2.3.1. Calculation of Specific Humidity

Specific humidity of radiosonde stations need to be calculated by the following formulas. Firstly, dew point temperature T_d (°C) is obtained through dew point temperature difference, Δt (°C), and air temperature, t (°C). Secondly, actual water vapor pressure, e (hPa), is calculated according to the Magnus empirical formula. Finally, specific humidity, q (g/kg), is derived from the two elements of water vapor pressure and atmospheric pressure, P (hPa), in combination with the equation of wet air state [30]:

$$T_d = t - \triangle t \tag{1}$$

$$e = 6.11 \times 10^{\frac{7.45 \times T_d}{235 + T_d}} \tag{2}$$

$$q = 622 \frac{e}{P} \tag{3}$$

2.3.2. Evaluation of Specific Humidity

In this study, we compared the differences in terms of value and dispersion between radiosonde data and reanalysis data by the following three formulas. To some extent, it can represent the potential ability to estimate and replace radiosonde data from reanalysis data [31].

The mean difference ($\overline{D}$) (4) between reanalysis and observation data represents the average difference in specific humidity during the period 1980–2013. The root mean square error (RMSE) (5) is used to reflect the deviation of reanalysis data from observation data. The correlation coefficient (COR) between reanalysis and observation data is defined as Formula (6):

$$\overline{D} = \frac{\sum_{i=1}^{n} |y_i - x_i|}{n} \tag{4}$$

$$\text{RMSE} = \sqrt{\frac{\sum_{i=1}^{n} (y_i - x_i)^2}{n}} \tag{5}$$

$$\text{COR} = \frac{\sum_{i=1}^{n} (y_i - \overline{y})(x_i - \overline{x})}{\sqrt{\sum_{i=1}^{n} (y_i - \overline{y})^2} \sqrt{\sum_{i=1}^{n} (x_i - \overline{x})^2}} \tag{6}$$

where n is the number of stations, x_i, y_i and $\overline{x}$, $\overline{y}$ represent specific humidity and its mean value of reanalysis and observation data, respectively. A value of $\overline{D}$ that is close to 0, or a value of RMSE close to 0, or a value of COR close to 1, reflects a closer similarity between reanalysis and observation data.

2.3.3. Method of Trend Analysis

The linear trend of specific humidity is expressed as:

$$y_i = ax_i + b \tag{7}$$

where a is the regression coefficient, obtained by the least-squares method, which represents the long-term change characteristics. The nonparametric Mann–Kendall test is used to calculate Z statistics, and the Z-test table is used to judge whether the linear trend of change is significant. When the statistical value of Z is 0–1.96, this indicates that specific humidity change is not significant, when Z is 1.96–2.58, this indicates that specific humidity passes the significance test of 0.05, and when Z is greater than 2.58, this indicates that it passes the significance test of 0.01.

3. Results

3.1. Assessment of Reanalysis Data

The general characteristics of average statistics between ERA-interim and radiosonde data are similar to MERRA-2 and radiosonde data (Table 1). In terms of $\overline{D}$ and RMSE, the mean differences of ERA-interim and MERRA-2 are small, at the 850 hPa level, where $\overline{D}$ is 0.05 g/kg and 0.08 g/kg, and RMSE is 0.28 g/kg and 0.23 g/kg, respectively. At the 700–200 hPa levels, $\overline{D}$ and RMSE show the same characteristics that the highest value appears at 700 hPa and the lowest at 200 hPa. The reason for this is that, with the increase of altitude, water vapor content decreases gradually, actual water vapor pressure decreases, and the specific humidity decreases. The trend of COR in the vertical atmospheric levels is different between $\overline{D}$ and RMSE, which shows the smallest COR at 200 hPa. It is worth noting that COR is always over 0.75 at the 850–300 hPa levels, which reaches the maximum at 500 hPa, about 0.98 and 0.99 of ERA-interim and MERRA-2, respectively.

Table 1. General characteristics of average statistics between ERA-interim, MERRA-2 and radiosonde data.

Level (hPa)	**ERA-Interim**			**MERRA-2**		
	$\overline{D}$ **(g/kg)**	**RMSE (g/kg)**	**COR**	$\overline{D}$ **(g/kg)**	**RMSE (g/kg)**	**COR**
200	0.02	0.02	0.27	0.01	0.01	0.26
300	0.03	0.03	0.87	0.03	0.03	0.75
400	0.10	0.11	0.95	0.12	0.12	0.96
500	0.20	0.22	0.98	0.25	0.25	0.99
700	0.36	0.43	0.88	0.40	0.41	0.95
850	0.05	0.28	0.94	0.08	0.23	0.94

3.2. Temporal Variation and Linear Trend of Tropospheric Specific Humidity

Due to the low correlation between reanalysis data and radiosonde data at 200 hPa, as well as the fact that there are fewer radiosonde stations after quality control at 850 hPa because of the high altitude in the Tianshan Mountains and other places, 300 hPa, 400 hPa, 500 hPa, and 700 hPa levels have been selected to analyze the temporal trend of specific humidity. It had been noted that the radiosonde data in China underwent an instrument type change in the early 2000s; the humidity sensor was abnormally dry with only a slight rise in the lower troposphere [32,33]. As shown in Figure 2, specific humidity dropped sharply at 500–300 hPa after 2006 in the arid region of northwest China. Therefore, it is necessary to correct and interpolate the specific humidity of radiosonde stations after 2006.

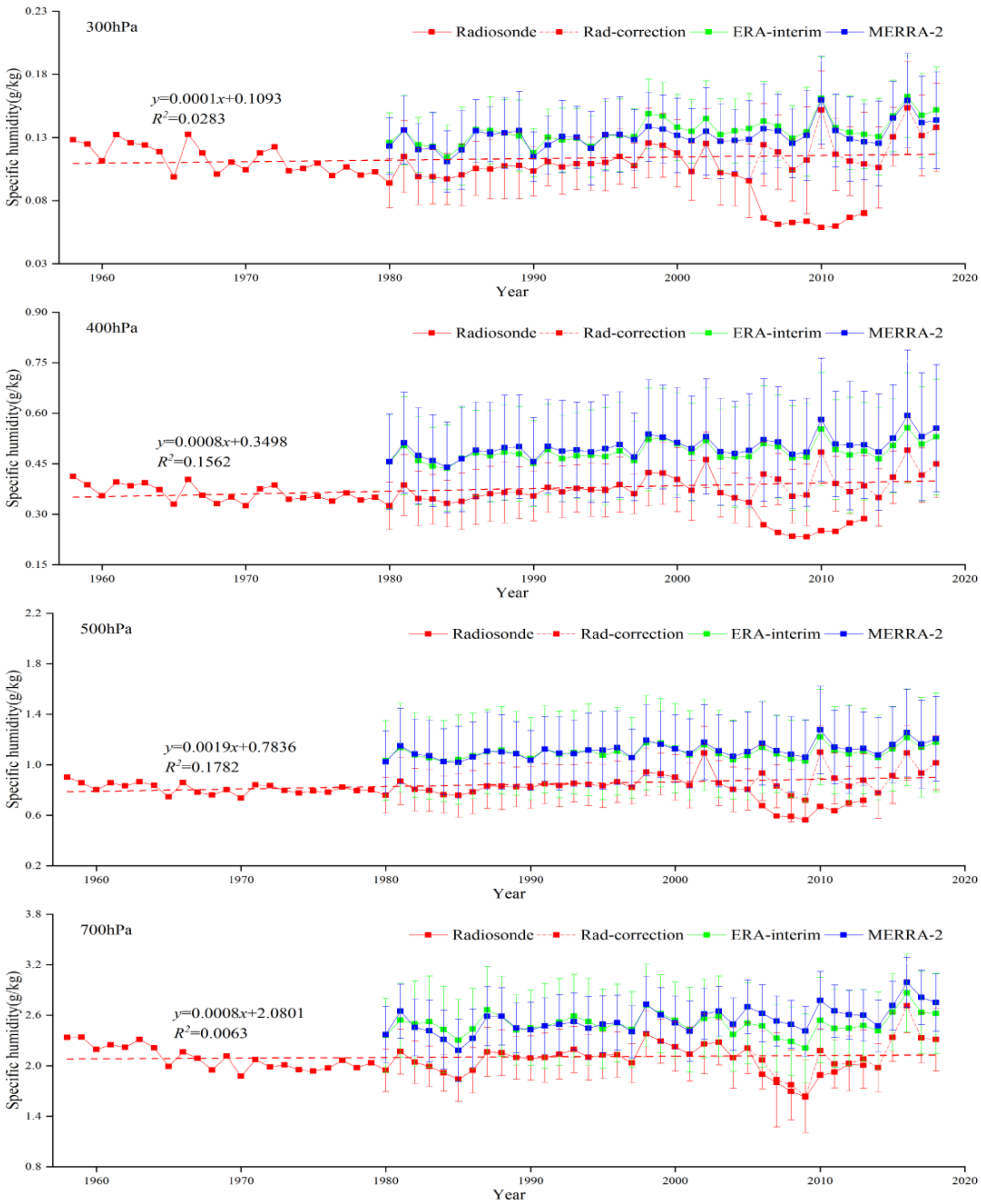

Figure 2. Temporal variation and linear trends of annual average specific humidity of various pressure-latitudes over the region during the period 1958–2018.

From the figure relating to temporal variation and linear trends of annual average specific humidity (Figure 2), it can be seen that three sets of data have relatively consistent changes during the period from 1980 to 2018. In terms of values, radiosonde data are lower than the reanalysis data. ERA-interim and MERRA-2 are closer to each other, in respect of both trend and values. For the radiosonde data, the annual specific humidity of the four mandatory levels from 1958 to 2018 shows a positive trend, and the positive trend is not significant at 300 hPa and 700 hPa, increasing by 0.001 g/(kg·10a) and 0.008 g/(kg·10a), respectively. On the contrary, the annual specific humidity has a positive trend at 99% confidence level at 400 hPa and 500 hPa, with an increase of 0.008 g/(kg·10a) and 0.019 g/(kg·10a), respectively. In the arid region of northwest China, temporal variation presents the characteristic of stage change in the tropospheric specific humidity from 1958 to 2018; taking the middle of the 1980s and 2002 as boundaries, all four mandatory levels show the trend of "declining-gentle rising-fluctuation rising". The gentle rise in the mid-1980s may be related to the strong signal of a warmer and wetter climate from 1987 in the western Tianshan Mountains, as proposed by Shi et al. [34].

In Figure 3, the seasonal average specific humidity of various pressure levels during the period 1958–2018 is shown. In the arid region of northwest China, due to the high temperature, abundant precipitation, and accumulation of tropospheric water vapor in summer, specific humidity has a significant influence on the annual specific humidity. Therefore, when we analyze the seasonal linear trend, the trend of summer is mainly discussed in stages. The change of specific humidity in summer on the mandatory level at 700–300 hPa is synchronous, showing a process of "declining-gentle rising-fluctuation rising". The specific process of change can be divided into three stages. The first stage is the period of 1958–1985, where the specific humidity shows a fluctuating decreasing trend. The decreasing rate is most obvious at 700 hPa, with an average decrease of 0.15 g/(kg·10a), and the decreasing rate at 500 hPa is lower than other levels. The second stage is the period of 1986–2000; the specific humidity shows a rapid and steady increasing trend. The third stage is the period of 2001–2018; the specific humidity shows a fluctuating increasing trend, with a rising rate of 700 hPa > 500 hPa > 400 hPa > 300 hPa, which varies with altitude. With the elevation increasing, the water vapor pressure decreases, and the rising rate of specific humidity gradually decreases. In the four seasons, the amount of humidity in the atmosphere is reduced in the order of summer, autumn, spring, winter. In terms of the rate of change, the specific humidity of spring, autumn, and winter is lower than summer.

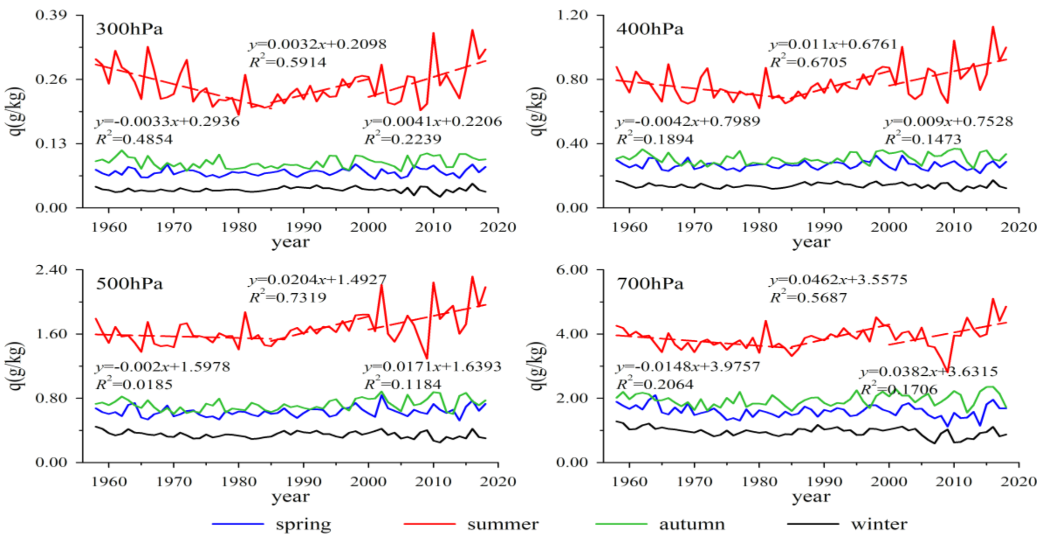

Figure 3. Temporal variation and linear trend of annual average specific humidity of various pressure-latitudes over the region during the period 1958–2018.

3.3. Multi-Year Mean Tropospheric Specific Humidity and Trends

Due to the high correlation between the two sets of reanalysis data and the similar variation trends and values, only the ERA-interim data is used to analyze the monthly mean specific humidity of each vertical pressure level in the arid region of northwest China (Figure 4). The maximum value of the monthly mean specific humidity of different mandatory levels is at the lower level (850–700 hPa). The highest value appears in the warm and wet months of the year from June to August, in which the specific humidity is between 4 and 6 g/kg. The lowest value appears in the cold months from December to February in the next year, in which the humidity is between 0.9 to 1.4 g/kg. At the middle level (500–400 hPa) and upper level (300–200 hPa), the highest and lowest value of specific humidity appears in the same month, which is consistent with the lower troposphere, and the value becomes smaller as the pressure altitude increases. From the lower to the upper layer of the atmosphere, the most vertical expansion in specific humidity is in July, followed by June and August. With the decreasing temperature, the specific humidity vertical expansion is decreased during the period March–May and September–November; the smallest vertical expansion appears in December to February.

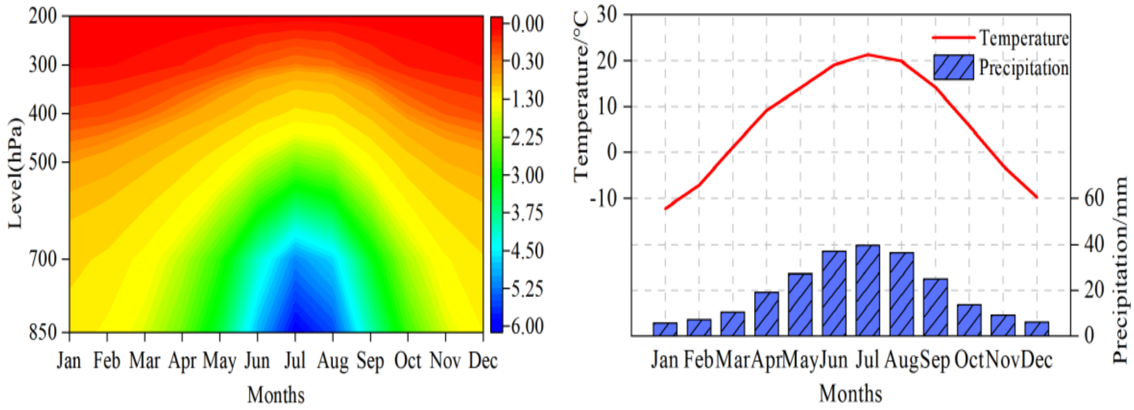

Figure 4. Level-month profile of annual specific humidity and monthly average temperature and precipitation during the period 1980–2018.

Figure 5 shows well the vertical profiles of annual and seasonal specific humidity and linear trends of the study area during the period 1980–2018. The annual and seasonal average specific humidity outlines of radiosonde (1a) show that the specific humidity is 5.8 g/kg in summer due to a series of strong convective activities at the lower levels, and the specific humidity gradually becomes lower towards the upper troposphere, with 0.065 g/kg. In other seasons, the convective activity is weak and the specific humidity is smaller than that in summer. The two sets of reanalysis data (2a, 3a) show good consistency with the radiosonde data in the vertical profile of specific humidity with altitude. However, the data from the radiosonde and the two sets of reanalysis have slight changes in numerical values, which shows that the annual and seasonal mean specific humidity of the radiosonde station data are larger than that of the reanalysis data at 200 hPa and 850 hPa, while the opposite trend is observed at 700–300 hPa; the reanalysis data has larger specific humidity. The reason for this result is related to the low correlation between reanalysis data and radiosonde data at 200 hPa and fewer radiosonde stations at 850 hPa.

The linear trend outlines of specific humidity of radiosonde (Figure 5(1b)) indicate that the annual, summer, and autumn specific humidity show an upward trend at each vertical pressure level in the arid region of northwest China. In winter, all the pressure levels show a decreasing trend, except for the 200 hPa level. There is an increasing trend in the lower levels and a decreasing trend in the upper levels in spring. From Figure 5(2b,3b), the two sets of reanalysis data show a consistent rising trend in summer and autumn; the reanalysis data differs greatly in showing the linear trend of specific humidity in spring and winter, not only in the positive and negative trends of specific humidity but also in the rate of the trend. For the two sets of reanalysis data, ERA-interim and radiosonde data have a more consistent trend than MERRA-2.

3.4. Distribution of Spatial Variation and Linear Trend of Tropospheric Specific Humidity

Figure 6 represents the spatial distribution of annual mean specific humidity at different atmospheric levels in the arid region of northwest China from 1980 to 2018. The amount of interpolated radiosonde specific humidity is lower than the reanalysis data. At the lower levels, at 850–700 hPa, the spatial distribution of specific humidity is characterized by "high in the east and west and low in the middle". The Yili River Valley of the Western Tianshan Mountains is the windward slope of the westerly currents, where the direction of topography intercepts a large amount of water vapor for this area. Therefore, the amount of specific humidity is high. In the central and south of the study area, which has basins and desert features in the terrain, the amount of specific humidity is low due to the high temperature, less water vapor, and strong evaporation, which accounts for only 1/4–1/3 of the Yili River Valley. The Qilian Mountains, located in the southeast of the region and influenced by westerly water vapor and the summer monsoon, the specific humidity is high. At the middle and upper levels, both the radiosonde stations and the reanalysis data are consistent with a gradual decrease trend of specific humidity from south to north. At 500–300 hPa, the distribution of the specific humidity amount is influenced by the westerly water vapor and latitude, not by the topography and underlying surface, and the maximum specific humidity is observed over the southwest and south of the area.

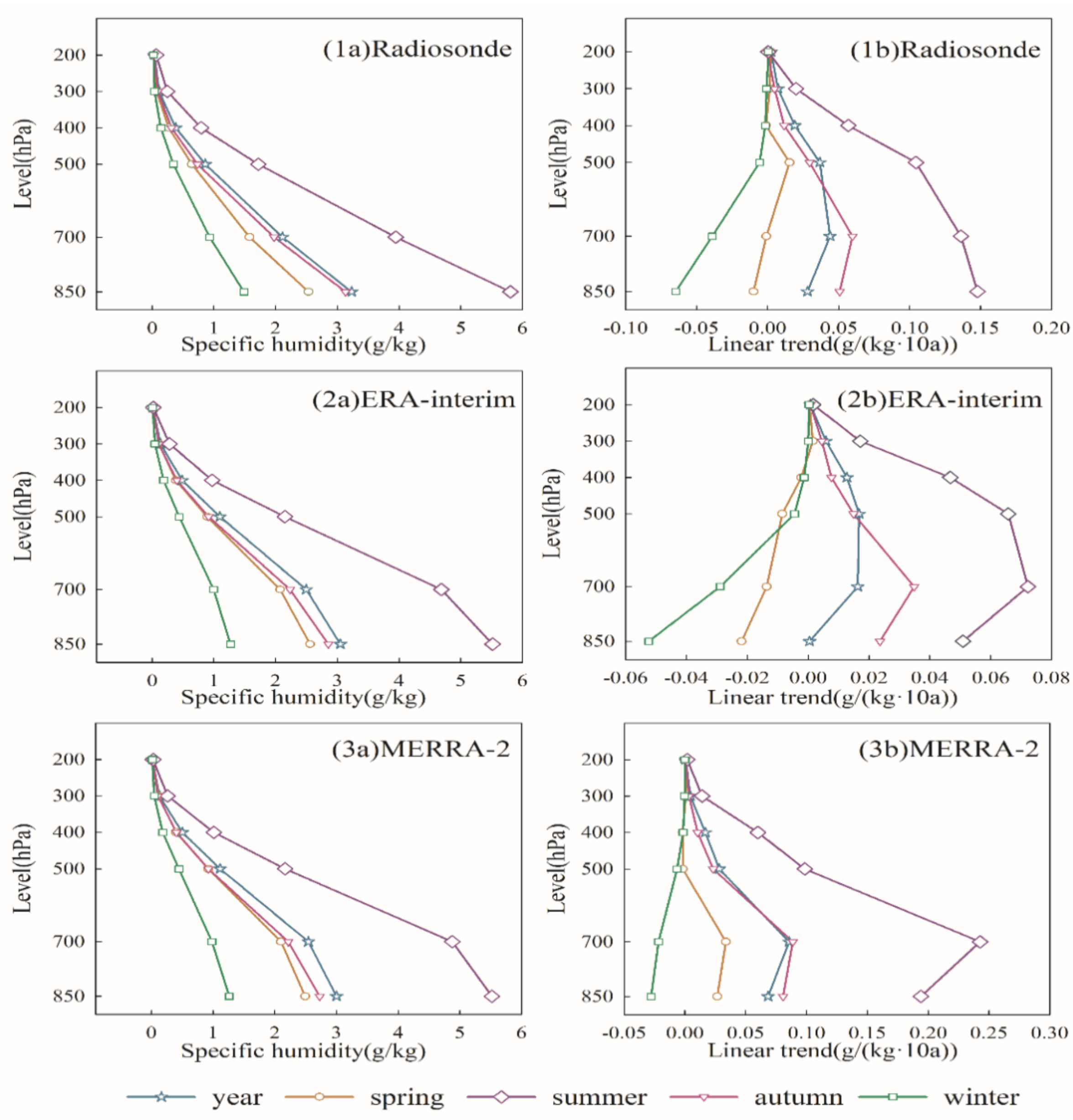

Figure 5. Vertical profiles of annual and seasonal specific humidity (**1a**,**2a**,**3a**) and linear trends (**1b**,**2b**,**3b**) of area average during the period 1980–2018.

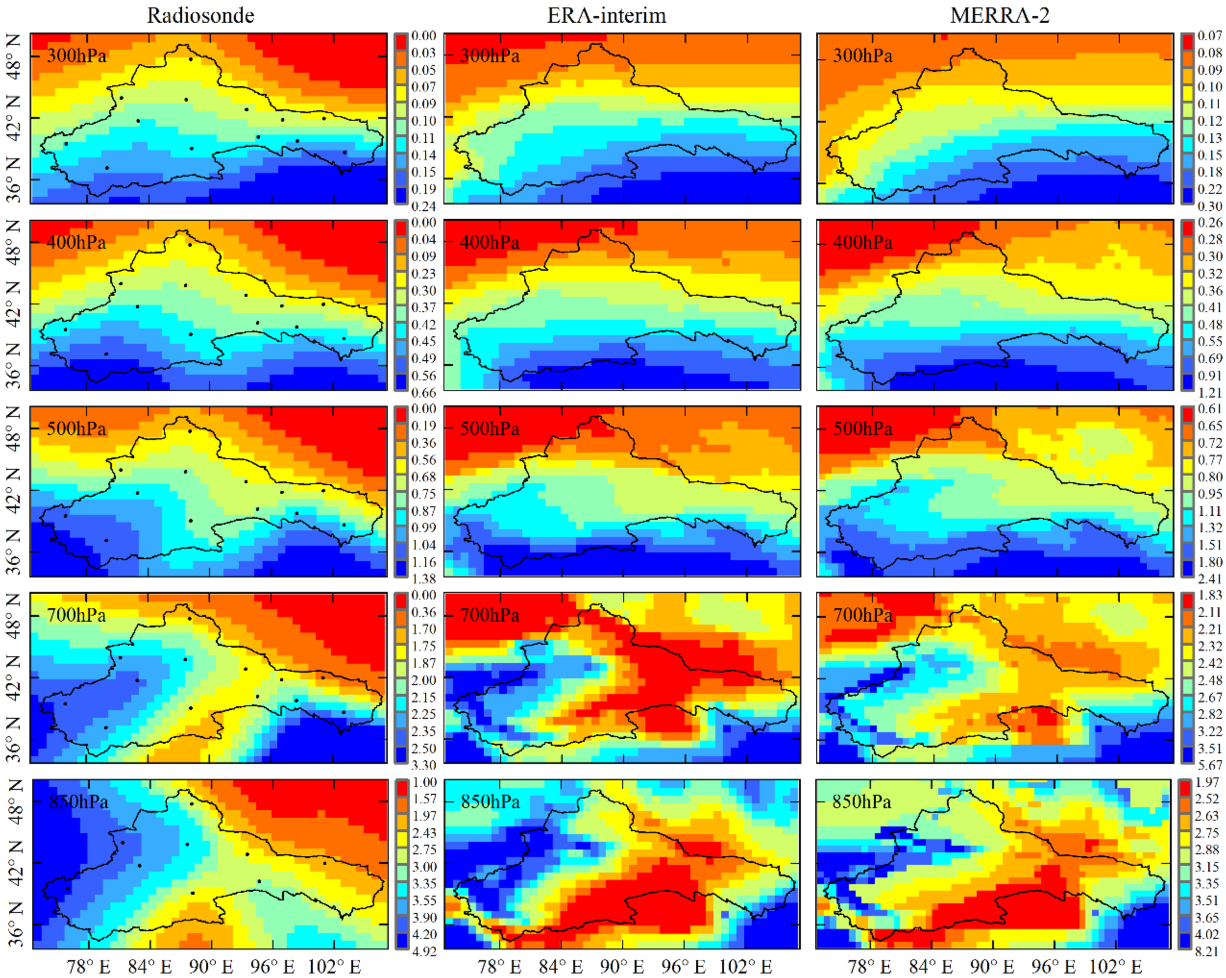

Figure 6. The long-term mean spatial distribution of specific humidity (g/kg) in different atmospheric levels during the period 1980–2018.

The vertical profiles of the zonal and meridian long-term average of specific humidity (g/kg) at the 850–200 hPa levels are shown in Figure 7. From latitude-level, the maximum specific humidity is 3.3–3.8 g/kg at 850–700 hPa. There are three peak areas of specific humidity along the zonal distribution, which are located at 34–37° N, 41–45° N, and 47–50° N. Interestingly, these peak areas are consistent with the distribution of the three mountains in the arid region of northwest China, from the south to the north: the Kunlun Mountains, the Tianshan Mountains, and the Altai Mountains. The mountains have widened further along the vertical direction. At 500–200 hPa, the distribution of the specific humidity amount is hardly influenced by the topography and underlying surface. By moving from the south to the north, the amount of specific humidity gradually decreases in the study area, and the changes in the lower levels are significant. Towards the upper-tropospheric levels, the specific humidity is more stable than at other levels. For the 850–700 hPa from longitude-level, the maximum specific humidity is located in the Kunlun Mountains and the western Tianshan Mountains at 74 °E, and the extent of this massive humidity distribution extends to 81 °E. Wang et al. [10] found that the atmosphere in the westerly belt formed a water vapor sink after 1979, and water vapor gathered on the windward slope when encountering high mountains. In addition, due to the proximity to the eastern monsoon region of China and affected by westerly water vapor, the core of the maximum specific humidity is 4.14 g/kg, which is located at 102–107° E. The specific humidity does not change significantly along the longitude at 500–200 hPa.

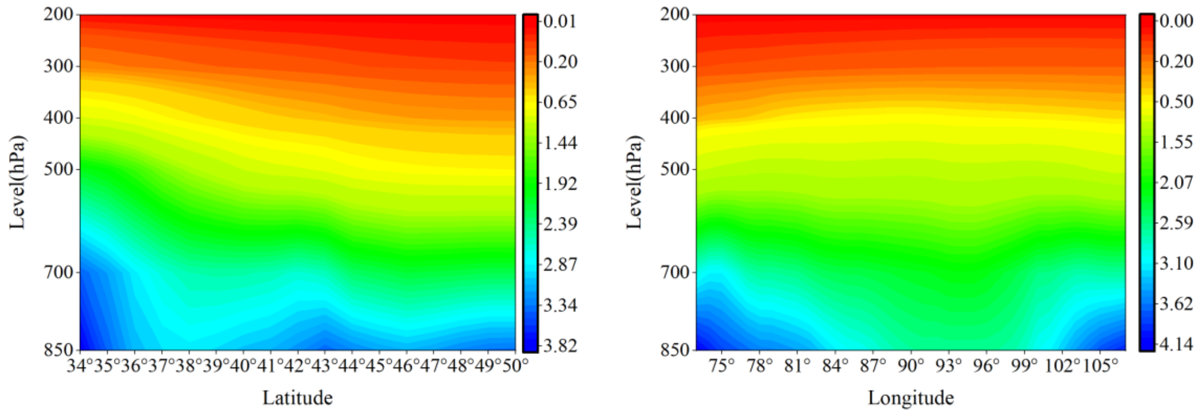

Figure 7. Vertical profiles of zonal and meridian average of specific humidity (g/kg) in different atmospheric levels during the period 1980–2018.

To study the trend of specific humidity from different atmospheric levels during the period 1980–2018 in the arid region of northwest China, the spatial distribution of the trends between station data and grid point data was analyzed, as shown in Figure 8. At 700 hPa, a negative trend of specific humidity is observed at Aletai, Kashgar, Mazongshan and Hami, and a positive trend is observed at other stations. However, only the four stations in the east have a positive trend at 95% confidence level. The two sets of reanalysis data at the 700 hPa level differ significantly from the radiosonde data, and their similarity is poor. At the levels of 500–400 hPa, the specific humidity of the station in the northwest shows a negative trend, and the others shows a positive trend. The increasing trend in the east of the study area is more significant than that in the west. The spatial distribution characteristics of the trend are roughly similar between the two sets of reanalysis data. At 300 hPa, the specific humidity at all stations shows a weak trend, and most stations have a positive trend. The two sets of reanalysis data well depict the increasing characteristics of specific humidity in the arid region of northwest China from 1980 to 2018, and the specific humidity of radiosonde stations is smaller than the reanalysis data. In general, the spatial distribution of the trends of specific humidity is well described by the two sets of reanalysis data at the middle and upper levels, but there are some deficiencies in depicting the trends in the lower levels.

3.5. Discussion

The above analysis reveals that the temporal and spatial variation of specific humidity and its distribution characteristics are not only affected by factors such as temperature, precipitation, underlying surface, and topography features, but are also influenced by the climatic state of the wind field. The wind field at 300, 500, 700, and 850 hPa levels in the atmosphere from 1980 to 2018 (Figure 9) reveals that the wind speed gradually strengthens with the increasing altitude. In the lower troposphere, due to the influence of the northwesterly dry and cold wind from Siberia, the specific humidity is low in the central and northern part of the arid region of northwest China. At the 700 hPa level, there is a high specific humidity area in the Yili River Valley. Warm and wet water vapor from the Atlantic Ocean is blocked by the Tianshan Mountains, and the underlying surface is oasis, which makes the specific humidity higher than in other areas. At the 500–300 hPa level, the effect of the westerly jet is strong, and the effect of the ground system becomes insignificant to both the wind field and the specific humidity.

The two sets of reanalysis data, ERA-interim and MERRA-2, can well depict the spatial and temporal distribution of specific humidity. However, due to the small number of radiosonde stations and their uneven distribution, the estimation value of reanalysis data is larger than the observation data. Affected by many unstable factors, there are some differences in showing the spatial distribution of the trends of specific humidity in the lower layers. Reanalysis data integrates numerical forecast products and observation data by using data assimilation techniques, which necessarily includes errors introduced by changes in numerical models, assimilation schemes, and observation systems. Additionally, the reanalysis data cannot completely replace observation data to describe the three-dimensional state of the atmosphere and reflect the long-term climate change trends. Therefore, it is important to evaluate the applicability of the data in the study area before applying the reanalysis data.

At 850 hPa, there are not any missing values of reanalysis data in the higher elevation mountainous areas. Therefore, the ground pressure, to avoid introducing false specific humidity on the ground, must be considered when calculating the water vapor content by integrating the specific humidity levels; this was also mentioned in the study on the Tibetan Plateau by Zhao et al. [35]. However, our study does not provide a specific quantitative analysis of the effects of temperature, precipitation, and climatic drought indices on specific humidity, which we will discuss in the next research.

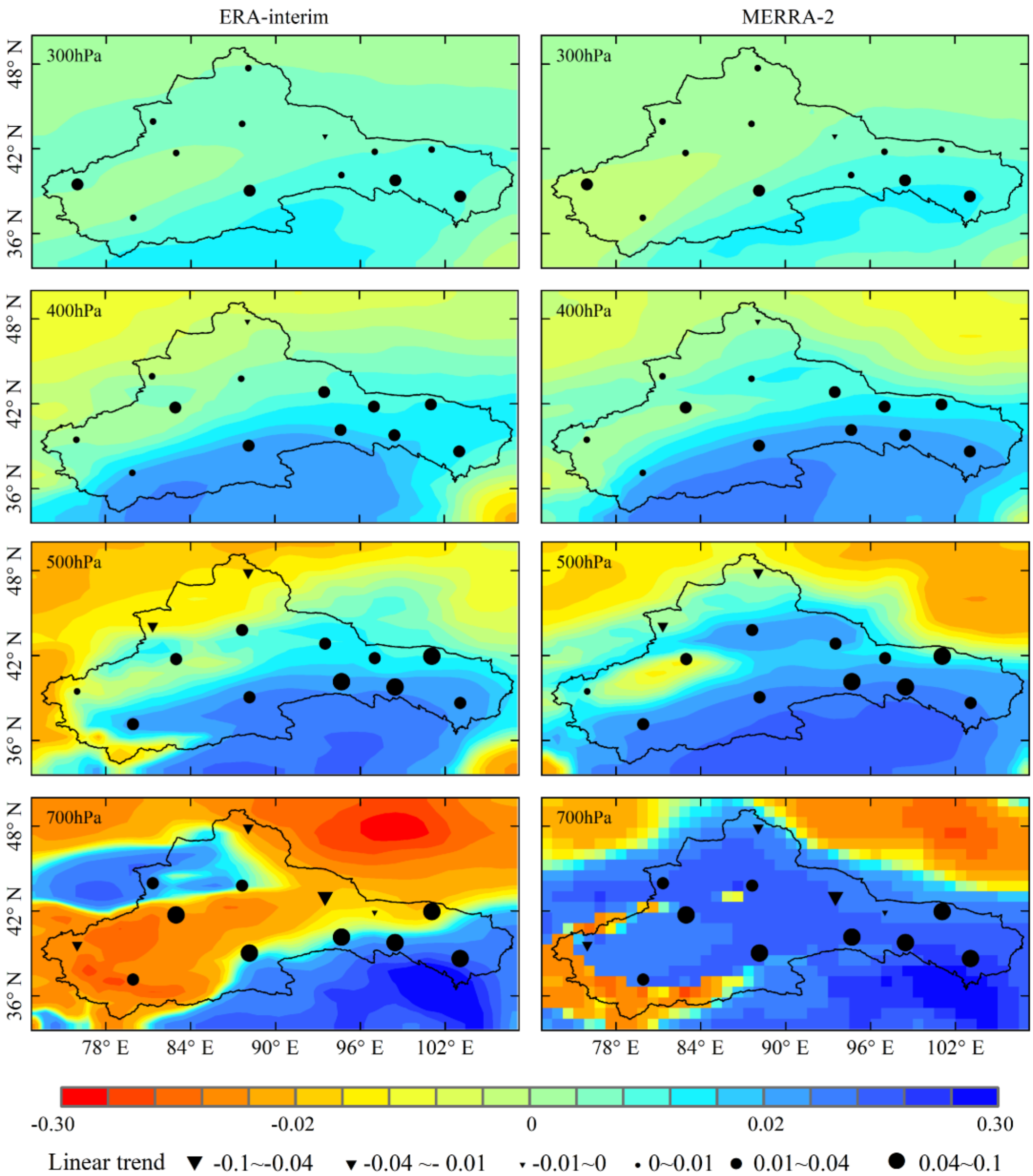

Figure 8. Spatial distribution of the trends of specific humidity from different atmospheric levels during the period 1980–2018 (g/(kg·10a)).

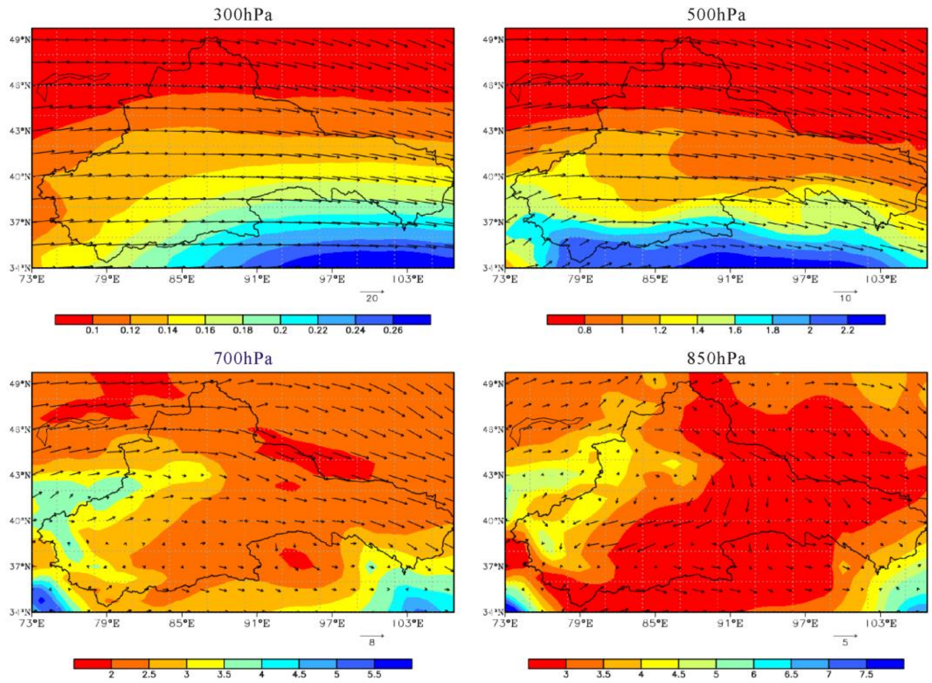

Figure 9. The long-term mean spatial distribution of the wind field at different atmospheric levels during the period 1980–2018.

4. Conclusions

In this paper, the temporal and spatial distribution of specific humidity at different levels of the atmosphere in the arid region of northwest China was studied, based on the radiosonde data and reanalysis data.

Firstly, we evaluated the two sets of reanalysis data. The correlation coefficient between radiosonde and two sets of reanalysis data is high, indicating that the reanalysis data can represent the potential ability to estimate radiosonde data in terms of change characteristics of specific humidity in the arid region of northwest China.

Secondly, in terms of radiosonde, the annual and summer specific humidity both show a positive trend in the vertical atmospheric levels. Taking the middle of the 1980s and 2002 as boundaries, the four levels show the trend of "declining-gentle rising-fluctuation rising". Due to the high temperature, abundant precipitation, and accumulation of tropospheric water vapor in summer, specific humidity has a significant influence on the annual specific humidity. From the lower atmospheric layer to the upper, the most vertical expansion in specific humidity is in July. The amount of humidity in the atmosphere is reduced in the order of summer, autumn, spring, winter. The three sets of data consistently show that the annual, summer, and autumn specific humidity show an upward trend at each vertical pressure level in the arid region of northwest China, and ERA-interim and radiosonde data have a more consistent trend than MERRA-2.

Finally, the spatial distribution of specific humidity in the lower levels is greatly influenced by the topography and underlying surface and the maximum specific humidity is observed over the Yili River Valley of the Western Tianshan Mountains and the Qilian Mountains. However, there is a gradual decrease trend in specific humidity from south to north in the middle and upper levels. In terms of the spatial distribution of the linear trend of specific humidity, most of the negative trend is observed at 700 hPa, and a positive trend is observed at other levels. The spatial distribution of the trends of specific humidity is well described by the two sets of reanalysis data at the middle and upper levels, but there are some deficiencies in depicting the trend at the lower levels.

Author Contributions: Data curation, M.S. and X.Y.; formal analysis, H.Z.; methodology, H.Z.; writing—original draft, H.Z.; writing—science advising, review, and editing, M.S., Z.W., and

L.Z.; funding acquisition, M.S.; All authors have read and agreed to the published version of the manuscript.

Funding: This research was funded by the National Natural Science Foundation of China, grant numbers 41801052 and 41861013.

Institutional Review Board Statement: Not applicable.

Informed Consent Statement: Not applicable.

Data Availability Statement: Publicly available datasets were analyzed in this study. This data can be found here: The radiosonde data was available online from http://data.cma.cn (accessed on 1 September 2020). The ERA-interim reanalysis data was available online from https://apps.ecmwf.int/datasets/data/interim-full-daily (accessed on 1 September 2020). The MERRA-2 reanalysis data was available online from https://disc.gsfc.nasa.gov/datasets?keywords=MERRA-2 (accessed on 1 September 2020).

Acknowledgments: We thank the China Meteorological Data Service Center, European Centre and NASA for the data. We also gratefully thank the reviewers.

Conflicts of Interest: The authors declare no conflict of interest.

References

1. Liu, G.W. *Atmosphere Process in Hydrologic Cycle*; Science Press: Beijing, China, 1997.
2. Brown, P.J.; Degaetano, A.T. Trends in U.S. surface humidity, 1930–2010. *J. Appl. Meteorol. Clim.* **2013**, *52*, 147–163. [CrossRef]
3. Dessler, A.E.; Sherwood, S.C. A matter of humidity. *Science* **2009**, *323*, 1020–1021. [CrossRef]
4. Dominguez, F.; Kumar, P.; Liang, X.Z.; Ting, M. Impact of atmospheric moisture storage on precipitation recycling. *J. Clim.* **2006**, *19*, 1513–1530. [CrossRef]
5. He, J.H.; Guo, P.W.; Yin, Y.; Shen, S.W. *Introduction of Atmospheric Science*; China Meteorological Press: Beijing, China, 2015; pp. 34–45.
6. Gong, N.G.; Sun, M.P.; Yan, L.X.; Gong, P.; Ma, X.G.; Mou, J.X. Temporal and spatial characteristics of atmospheric water vapor and its relationship with precipitation in Qilian Mountains during 1979–2016. *Arid Land Geogr.* **2017**, *40*, 762–771. [CrossRef]
7. Wang, K.; Sun, M.P.; Gong, N.G. Spatial and temporal distribution and transportation of the water vapor in the Northwestern China. *Ari. Land Geogr.* **2018**, *41*, 290–297. [CrossRef]
8. Zhang, Y.; Li, B.F.; Chen, Y.N. The temporal and spatial Variation of water vapor content and its relationship with precipitation in the arid region of Northwest China from 1970 to 2013. *J. Nat. Resour.* **2018**, *33*, 1043–1055. [CrossRef]
9. Igbawua, T.; Zhang, J.H.; Yao, F.M.; Zhang, D. Assessment of moisture budget over West Africa using MERRA-2's aerological model and satellite data. *Clim. Dyn.* **2018**, *52*, 83–106. [CrossRef]
10. Wang, B.J.; Huang, Y.X.; Tao, J.H.; Li, D.L.; Wang, P.X. Regional Features and Variations of Water Vapor in Northwest China. *J. Glaciol. Geocryol.* **2006**, *28*, 15–21.
11. Bosilovich, M.G.; Robertson, F.R.; Chen, J.Y. Global Energy and Water Budgets in MERRA. *J. Clim.* **2011**, *24*, 5721–5739. [CrossRef]
12. Xu, D.; Kong, Y.; Wang, C.H. Changes of water vapor budget in arid area of Northwest China and its relationship with precipitation. *J. Arid Meteorol.* **2016**, *34*, 431–439.
13. Qiu, S.; Zhou, W.; Leung, M.Y.; Li, X.Z. Regional moisture budget associated with drought/flood events over China. *Prog. Earth Planet. Sci.* **2017**, *4*, 36. [CrossRef]
14. Tao, C.; Zhang, Y.Y.; Tang, S.Q.; Tang, Q.; Ma, H.; Xie, S.C.; Zhang, M.H. Regional moisture budget and land–atmosphere coupling over the US Southern Great Plains inferred from the ARM long–term observations. *J. Geophys. Res. Atmos.* **2019**, *124*, 10091–10108. [CrossRef]
15. Chen, Y.; Li, Y.Q.; Fan, G.Z.; Chen, Y.H. Study on temporal spatial distribution characteristics of latent heat over the Qinghai–Tibetan Plateau. *Plateau Meteorol.* **2019**, *38*, 460–473.
16. Yao, J.Q.; Chen, Y.N.; Zhao, Y.; Guan, X.F.; Mao, W.Y.; Yang, L.M. Climatic and associated atmospheric water cycle changes over the Xinjiang, China. *J. Hydrol.* **2020**, *585*, 124823. [CrossRef]
17. Dessler, A.E.; Davis, S.M. Trends in tropospheric humidity from reanalysis systems. *J. Geophys. Res. Atmos.* **2010**, *115*, D19127. [CrossRef]
18. Darand, M.; Pazhooh, F.; Saligheh, M. Trend analysis of tropospheric specific humidity over Iran during 1979–2016. *Int. J. Climatol.* **2019**, *39*, 4058–4071. [CrossRef]
19. Zhang, S.Q.; Guo, Y.J.; Wang, G.F. A comparative study of atmospheric humidity over China between radiosonde and the third generation reanalysis datasets. *Acta Meteorol. Sin.* **2018**, *76*, 289–303. [CrossRef]
20. Guo, Y.J.; Ding, Y.H. Upper-air specific humidity change over China during 1958–2005. *Chin. J. Atmos. Sci.* **2014**, *38*, 1–12.
21. Xu, B.R.; Zou, S.B.; Du, D.Y.; Xiong, Z.; Lu, Z.X.; Ruan, H.W.; Xiao, H.L. Variation of tropospheric specific humidity upon the middle-lower reaches of the Heihe River during 1981–2010. *J. Glaciol. Geocryol.* **2016**, *38*, 57–68.

22. Liu, Y.Y.; Li, Y.F.; Xie, J.F.; Zhang, H. Climate change characteristics of free atmospheric humidity and its relationship with temperature and precipitation in Northeast China. *Sci. Geogr. Sin.* **2016**, *36*, 628–636. [CrossRef]
23. Zhao, S.Q. A new scheme for comprehensive physical regionalization in China. *Acta Geogr. Sin.* **1983**, *38*, 1–10.
24. Zhang, Q.; Hu, Y.Q.; Cao, X.Y.; Liu, W.M. On Some Problems of Arid Climate System of Northwest China. *J. Des. Res.* **2000**, *20*, 13–18.
25. Chen, Y.N.; Yang, Q.; Luo, Y.; Shen, Y.J.; Pan, X.L.; Li, L.M.; Li, Z.Q. Ponder on the issues of water resources in the arid region of Northwest China. *Arid Land Geogr.* **2012**, *35*, 1–9. [CrossRef]
26. Chen, D.D.; Zhao, J. Spatial–temporal variation of lake area in arid region of Northwest China. *Remote Sens. Tech. Appl.* **2017**, *32*, 1114–1125.
27. Dee, D.P.; Uppala, S.M.; Simmons, A.J.; Berrisford, P.; Poli, P.; Kobayashi, S.; Andrae, U.; Balmaseda, M.A.; Balsamo, G.; Bauer, P.; et al. The ERA-Interim reanalysis: Configuration and performance of the data assimilation system. *Q. J. R. Meteorol. Soc.* **2011**, *137*, 553–597. [CrossRef]
28. Wei, J.F.; Dirmeyer, P.A.; Bosilovich, M.G.; Wu, R.G. Water vapor sources for Yangtze River Valley rainfall: Climatology, variability, and implications for rainfall forecasting. *J. Geophys. Res.* **2012**, *117*, D05126. [CrossRef]
29. Gelaro, R.; Mccarty, W.; Suárez, M.J.; Todling, R.; Molod, A.; Takacs, L.; Randles, C.A.; Darmenov, A.; Bosilovich, M.G.; Reichle, R.; et al. The Modern-Era retrospective analysis for research and applications, Version 2 (MERRA–2). *J. Clim.* **2017**, *30*, 5419–5454. [CrossRef] [PubMed]
30. Lu, Y.R.; Gao, G.D. *Physical Climatology*; China Meteorological Press: Beijing, China, 1987.
31. Xiong, Q.F.; Huang, M.; Xiong, M.Q.; Hu, J.L. Cross-validation error analysis of daily gridded precipitation based on China meteorological observation. *Plateau Meteorol.* **2011**, *30*, 1615–1625.
32. Bian, J.C.; Chen, H.B.; VÖMEL, H.; Duan, Y.J.; Xuan, Y.J.; Lü, D.R. Intercomparison of humidity and temperature sensors: GTS1, Vaisala RS80, and CFH. *Adv. Atmos. Sci.* **2011**, *28*, 139–146. [CrossRef]
33. Hao, M.; Gong, J.D.; Wang, R.W.; Wan, X.M.; Liu, Y. The quality assessment and correction of the radiosonde humidity data biases of L-band in China. *Acta Meteorol. Sin.* **2015**, *73*, 187–199. [CrossRef]
34. Shi, Y.F.; Shen, Y.P.; Li, D.L.; Zhang, G.W.; Ding, Y.J.; Hu, R.J.; Kang, E.S. Discussion on the present climate change from warm-day to warm-wet in Northwest China. *Quat. Sci.* **2003**, *23*, 152–164.
35. Zhao, H.Y.; Zhang, X.Q.; Xie, C.Y. Applicability of reanalysis data of multi-source water vapor over the Tibetan Plateau. *Arid Zone Res.* **2017**, *34*, 300–308.